

Treatment of the Interface between Fine Elastic Structures and Fluids

N.D. Botkin, K.-H. Hoffmann, V.N. Starovoitov, V.L. Turova
 Center of Advanced European Studies and Research (caesar)
 Ludwig-Erhard-Allee 2, 53175 Bonn, Germany
 botkin@caesar.de, <http://www.caesar.de>

Abstract

The interaction of fine pin or bristle structures with fluids is studied. Such problems arise when modeling biomolecular layers moving in liquids or when simulating epithelium surfaces of blood vessels. We propose a homogenized model where the interaction between the bristles and the fluid is accounted through an averaged material whose properties are derived using the passage to the limit in the model based on the fluid-solid interface conditions as the number of the bristles goes to infinity whereas their thickness goes to zero. The model of such an averaged material is used for the study of a Love wave biosensor.

1 Introduction

This investigation is motivated by modeling a Love wave sensor based on the generation and detection of horizontally polarized shear waves (see [1] and Figure 1). Acoustic shear waves are excited due to an alternate voltage applied to electrodes deposited on a quartz crystal substrate. The waves are transmitted into a thin isotropic guiding layer covered by a thin gold film that contacts a liquid containing a protein to be detected. The protein adheres to a specific receptor, aptamer, immobilized on the surface of the gold film. The arising mass loading causes a phase shift in the electric signal to be measured by an electronic circuit.

One can impress the aptamer-protein layer as a periodic bristle structure on the top of the gold film contacting with the liquid (see Figure 2). The thickness of the aptamer-protein layer is about 4 nm and the number of bristles per surface unit is enormous large. Therefore, the direct numerical modeling of such a structure using fluid-solid interface conditions is impossible.

The two-scale homogenization technique (see [2, 3]) is used for the treatment of such an object. The bristle-fluid structure is replaced by an averaged ma-

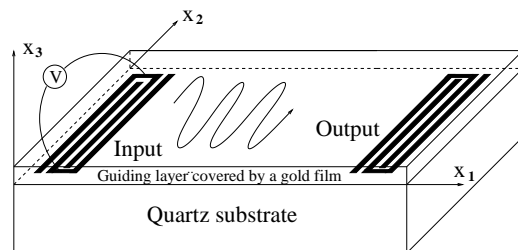


Figure 1: Draft of a Love wave biosensor

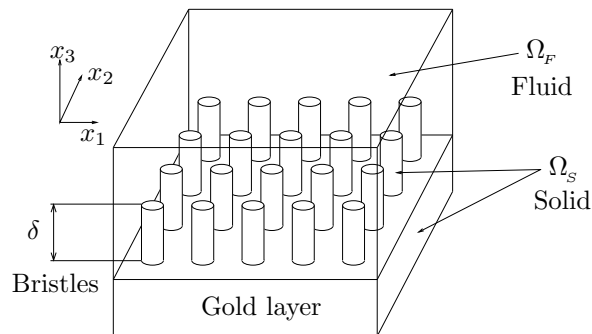


Figure 2: Coupled system: $\Omega = \Omega_F \cup \Gamma \cup \Omega_S$; Γ is the interface

terial whose properties are derived as the number of bristles goes to infinity whereas their thickness goes to zero. The fluid-solid interface conditions (see e.g. [4]) are accounted when passing to the two-scale limit. The height of the bristles remains constant.

The difference to known homogenized models like e.g. [5] proposed for the simulation of rigid rough surface-fluid interfaces consists in the assumption that the solid part is elastic. The fluid is assumed to be weakly compressible and the velocities in the fluid being sufficiently small. This enables the us-

age of the linearized Navier-Stokes equations. The motion of the solid is described by linear elasticity equations. On the fluid-solid interface, the continuity of normal pressures and velocities (no-slip condition) is assumed. The no-slip condition is the most hard to treat. We apply the approach proposed by J.-L. Lions in [6] which consists in the usage of the velocity instead of the displacement as the state variable for the solid. Using two-scale convergence, we obtain a limiting equation that describes a new material possessing some interesting properties: 1) the elastic modules decrease comparing to the ones of the bristle material but some resistance force which is proportional to the strain velocity appears; 2) the shear elastic modules become very small; 3) some short memory with respect to the strain arises. Thus, we obtain a thin layer made of a new material which contact the liquid from above and the solid body from below.

Using the model of the new material, we compute dispersion relations which express the dependence of the Love wave velocity on the excitation frequency. Based on the dispersion relations, one can compute many useful characteristics, for example, the sensitivity of the biosensor with respect to adhering ligand-biomolecules. Numerical algorithms developed by the authors work for any number of anisotropic layers. The precision of the method enables to estimate the sensitivity regarding nanoscopic mass loadings.

2 Mathematical Model

A coupled system modeling a periodic bristle or pin structure contacting with a fluid is shown in Figure 2. The solid part consists of a substrate and pins located on its top. The pin structure is assumed to be periodic in (x_1, x_2) and independent of x_3 . The total domain of the coupled system is denoted by $\Omega \subset \mathbb{R}^3$. The domains occupied by the fluid and elastic continua are denoted by Ω_F and Ω_S , respectively; the boundary separating the continua is called Γ .

2.1 Equations for Fluid-solid Interface

The coupled system is described by the following equations

$$\rho_F \mathbf{v}_t = -\nabla p + \operatorname{div} P \mathbf{v}_x + \rho_F \mathbf{f} \quad \text{in } \Omega_F, \quad (1)$$

$$\gamma p_t = -\operatorname{div} \mathbf{v} \quad \text{in } \Omega_F, \quad (2)$$

$$\rho_S \mathbf{u}_{tt} = \operatorname{div} G \mathbf{u}_x + \rho_S \mathbf{f} \quad \text{in } \Omega_S. \quad (3)$$

The no-slip and pressure equilibrium conditions on

the fluid-solid interface read

$$\mathbf{u}_t = \mathbf{v} \quad \text{on } \Gamma, \quad (4)$$

$$G \mathbf{u}_x \cdot \mathbf{n} = (-pI + P \mathbf{v}_x) \cdot \mathbf{n} \quad \text{on } \Gamma, \quad (5)$$

whereas zero boundary and initial conditions are assumed for simplicity. Here, ρ_F and ρ_S are the densities of the fluid and the solid parts, respectively; \mathbf{v} is the velocity field of the fluid, p is the pressure in the fluid, \mathbf{u} is the displacement field of the solid part, \mathbf{f} is an external force like the gravity. The coefficient γ characterizes the compressibility of the fluid. The fourth-rank tensors P and G are of the following form

$$P \mathbf{v}_x = \lambda \operatorname{div} \mathbf{v} I + \mu D(\mathbf{v}), \quad G \mathbf{u}_x = l_1 \operatorname{div} \mathbf{u} I + l_2 D(\mathbf{u}).$$

The second-rank unit tensor I has the components $I_{ij} = \delta_{ij}$, where δ_{ij} is the Kronecker symbol. The strain velocity tensor $D(\mathbf{v})$ has, as usually, the components $D_{ij}(\mathbf{v}) = 1/2(\partial v_i / \partial x_j + \partial v_j / \partial x_i)$. The symbols λ and μ denote positive bulk and dynamic viscosity coefficients of the fluid, respectively; l_1 and l_2 are Lamé coefficients of the solid part if the solid phase is isotropic. As usually, the summation over repeating indices is assumed, \mathbf{n} denotes the normal vector to a surface or curve. Note that the components of the elastic stiffness tensor G can be arbitrary up to base restrictions so that arbitrary *anisotropic solids* can be considered.

The no-slip condition (4) is the main handicap for the mathematical treatment of the model (1)–(5). The method from [6] is used to overcome this difficulty by utilizing the velocity instead of the displacement in equation (3). This is being done by introducing the following integral operator

$$\mathcal{J}_t \mathbf{w} = \int_0^t \mathbf{w}(s) ds.$$

Now, equation (3) can be rewritten in the form

$$\rho_S \mathbf{v}_t = \operatorname{div} G \mathcal{J}_t \mathbf{v}_x + \rho_S \mathbf{f}, \quad (6)$$

where $\mathbf{v} = \mathbf{u}_t$. The pressure p can be expressed through the velocity \mathbf{v} from equation (3) as follows

$$p = -\gamma^{-1} \operatorname{div} \mathcal{J}_t \mathbf{v}. \quad (7)$$

2.2 Refinement of the Pin Structure

A refinement parameter ε will be introduced so that the value $\varepsilon = 1$ corresponds to the original structure but the number of pins grows, and the pins become finer whenever $\varepsilon \rightarrow 0$. Let χ be the characteristic function of the domain Ω_F . This function

will be redefined so that it becomes dependent on the refinement parameter. Assume that the (x_1, x_2) -projection of the base cell of the pin structure is a square and scale this square to the unit square $\Sigma = [0, 1] \times [0, 1]$. The (x_1, x_2) -projection of the solid part of the base cell will be transformed into a subset $\Sigma_S \subset \Sigma$. Denote the domain $\Sigma \setminus \overline{\Sigma_S}$ by Σ_F . The domain Σ is called structural cell (see Figure 3).

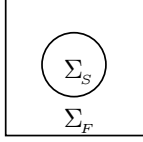


Figure 3: Structural cell $\Sigma = [0, 1] \times [0, 1]$

Let $\hat{\mathbf{x}} = (x_1, x_2)$ and $\hat{\chi}(\hat{\mathbf{x}})$ be the Σ -periodic extension of the characteristic function of the domain Σ_F to all \mathbb{R}^2 . We define the modified function χ^ε as follows (remember that δ is the thickness of the pin layer):

$$\chi^\varepsilon(\mathbf{x}) = \begin{cases} 1, & x_3 > \delta, \\ \hat{\chi}\left(\frac{\hat{\mathbf{x}}}{\varepsilon}\right), & -\delta \leq x_3 \leq \delta, \\ 0, & x_3 < -\delta. \end{cases} \quad (8)$$

Let us rewrite equations (1), (2), and (3) as one equation with discontinues coefficients in the whole domain Ω using the introduced characteristic function χ^ε . The equation reads

$$\rho^\varepsilon \mathbf{v}_t^\varepsilon = \operatorname{div} \mathbf{M}^\varepsilon \mathbf{v}_\mathbf{x}^\varepsilon + \rho^\varepsilon \mathbf{f}, \quad (9)$$

where

$$\begin{aligned} \rho^\varepsilon &= \rho_F \chi^\varepsilon + \rho_S (1 - \chi^\varepsilon), \\ \mathbf{M}^\varepsilon &= \chi^\varepsilon P + (\chi^\varepsilon \gamma^{-1} I \otimes I + (1 - \chi^\varepsilon) G) \mathcal{J}_t. \end{aligned}$$

The interface condition (4) is equivalent to the continuity of \mathbf{v}^ε on Γ but the condition (5) assumes now the form

$$G \mathcal{J}_t \mathbf{v}_\mathbf{x}^\varepsilon \cdot \mathbf{n} = (\gamma^{-1} \operatorname{div} \mathcal{J}_t \mathbf{v}^\varepsilon \cdot I + P \mathbf{v}_\mathbf{x}^\varepsilon) \cdot \mathbf{n} \quad \text{on } \Gamma^\varepsilon, \quad (10)$$

when accounting (7).

Theorem 1 *If $\mathbf{f}, \mathbf{f}_t \in L^2([0, T] \times \Omega)$, then a unique weak solution to problem (9), (10) satisfies the estimate*

$$\operatorname{ess\,sup}_{t \in (0, T)} (\|\mathbf{v}_t^\varepsilon(t)\|_{L^2(\Omega)} + \|\mathbf{v}_\mathbf{x}^\varepsilon(t)\|_{L^2(\Omega)}) \leq C, \quad (11)$$

where C is an independent of ε constant.

Theorem 1 ensures the existence of subsequences $\{\mathbf{v}^{\varepsilon_k}\}$ that converge to limiting functions \mathbf{v} . Using a two-scale convergence technique by G. Nguetseng and G. Allaire (see [7, 8], and [9]), one can show that all limiting functions satisfy the same limiting equation. From the uniqueness of solutions of the limiting equation, one concludes that the sequence \mathbf{v}^ε itself converges to an unique limiting function \mathbf{v} .

2.3 Limiting Equations

The two scale technique enables to derive the limiting equations. Nevertheless, the determination of their structure and computation of their coefficients is a challenge. Let Ω be divided into three parts

$$\begin{aligned} \Omega^f &= \{\mathbf{x} \in \Omega \mid x_3 > \delta\}, \\ \Omega^s &= \{\mathbf{x} \in \Omega \mid x_3 < -\delta\}, \\ \Omega^h &= \{\mathbf{x} \in \Omega \mid \delta < x_3 < -\delta\}. \end{aligned}$$

The limiting equations corresponding to the problem (9),(10) are of the form

$$\Omega^f : \rho_F \mathbf{v}_t - \operatorname{div} P \mathbf{v}_\mathbf{x} - \gamma^{-1} \nabla \operatorname{div} \mathcal{J}_t \mathbf{v} = \rho_F \mathbf{f}, \quad (12)$$

$$\Omega^s : \rho_S \mathbf{v}_t - \operatorname{div} \mathcal{J}_t G \mathbf{v}_\mathbf{x} = \rho_S \mathbf{f}, \quad (13)$$

$$\begin{aligned} \Omega^h : \rho_\theta \mathbf{v}_t - \operatorname{div} \overline{P} \mathbf{v}_\mathbf{x} - \operatorname{div} \mathcal{J}_t \overline{G} \mathbf{v}_\mathbf{x} \\ - \operatorname{div} \int_0^t \omega(t-s) \mathbf{v}_\mathbf{x}(s) ds = \rho_\theta \mathbf{f}. \end{aligned} \quad (14)$$

The physical conditions on the interfaces between Ω^h and Ω^f and between Ω^h and Ω^s are being derived from a preceding weak formulation that yields equations (12)–(14). Note, that equations (12) and (13) coincide with (1) and (6), respectively. Thus, the governing equations for the pure fractions remain unchanged by the homogenization, which has been of course expected. What we have new, is integral-differential equation (14) which can not be reduced to a pure differential equation by differentiating or by a substitution like $\mathbf{u} = \mathcal{J}_t \mathbf{v}$. The computation of the tensors \overline{P} , \overline{G} , and $\omega(\tau)$ is based on an analytical representation of solutions of the so-called cell equation which arises in homogenization theory. The difficulty is that the cell equation is not resolved with respect to the time derivative of the unknown function in our case. This handicap is overcome by restricting the cell equation to a certain subspace providing invertibility of the involved operators.

The computation of the tensors \overline{P} , \overline{G} , and $\omega(\tau)$ is being done with finite elements. The next theorem states their properties which provide the well-posedness of equation (14).

Theorem 2 *There exists a positive constant C such that*

$$\overline{P}_{ijkl} \mathcal{Z}_{ij} \mathcal{Z}_{kl} \geq C |\mathcal{Z}|^2, \quad \overline{G}_{ijkl} \mathcal{Z}_{ij} \mathcal{Z}_{kl} \geq 0$$

for every second-rank tensor \mathcal{Z} , where $|\mathcal{Z}|^2 = \mathcal{Z}_{ij}\mathcal{Z}_{ij}$. The tensor \bar{G} is degenerated, and $\bar{G}_{ijkl}\mathcal{Z}_{ij}\mathcal{Z}_{kl} = 0$ if and only if $\mathcal{Z}_{11} + \mathcal{Z}_{22} = 0$ and $\mathcal{Z}_{33} = 0$.

As one can see from equation (14), the tensor \bar{G} is the elastic stiffness tensor for the homogenized continuum. Theorem 2 says that the homogenized material has rather new properties. Namely, it does not resist to the deformation, if the first invariant and the component (3,3) of the corresponding strain tensor are equal to zero. In other words, such deformations do not produce any stresses. Such a class of deformations is sufficiently large: it contains all deformations which do not change the volume. Note that the tensor $\omega(\tau)$ falls very rapidly, if τ grows. The time scale is about 10^{-11} s for typical material parameters.

3 Dispersion Relations

Dispersion relations express the dependence of the wave velocity on the excitation frequency. Such a dependency is typical for multi-layered anisotropic structures like the biosensor. The computation of dispersion relations is based on the construction of traveling wave solutions that exponentially decrease towards $-x_3$ and $+x_3$ in the substrate and the fluid, respectively. Proper mechanical interface conditions between the layers as well as the interaction with the fluid have to be accounted.

For simplicity, consider a simplified structure shown in Figure 4 whose upper layer is free of liquid.

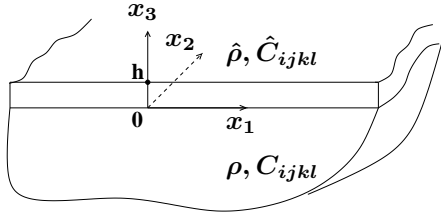


Figure 4: A sample structure. An anisotropic layer lies on an anisotropic half-space substrate. Here, $\hat{\rho}$, ρ , and \hat{C}_{ijkl} , C_{ijkl} are the densities and the elastic stiffness tensors, respectively

The elasticity equations for the substrate and the upper layer read:

$$\rho u_{i tt} - C_{ijkl} \frac{\partial^2 u_l}{\partial x_j \partial x_k} = 0, \quad i = 1, 2, 3, \quad (15)$$

$$\hat{\rho} \hat{u}_{i tt} - \hat{C}_{ijkl} \frac{\partial^2 \hat{u}_l}{\partial x_j \partial x_k} = 0, \quad i = 1, 2, 3, \quad (16)$$

where u_i and \hat{u}_i , $i = 1, 2, 3$, are components of the displacement vectors. A plain wave propagating in the structure in x_1 direction is of the form:

$$u_i(x_1, x_3) = a_i(x_3) \cos(kx_1 - \omega t) + b_i(x_3) \sin(kx_1 - \omega t), \quad (17)$$

$$\hat{u}_i(x_1, x_3) = \hat{a}_i(x_3) \cos(kx_1 - \omega t) + \hat{b}_i(x_3) \sin(kx_1 - \omega t). \quad (18)$$

Here, k is the wave value, ω the circuit frequency. The substitution of (17) and (18) into (15) and (16), respectively, yields

$$\begin{aligned} -C_{i33l} \ddot{a}_l - (C_{i13l} + C_{i31l}) \dot{b}_l + C_{i11l} a_l - \rho \frac{\omega^2}{k^2} a_i &= 0, \\ -C_{i33l} \ddot{b}_l + (C_{i13l} + C_{i31l}) \dot{a}_l + C_{i11l} b_l - \rho \frac{\omega^2}{k^2} b_i &= 0, \end{aligned}$$

and

$$\begin{aligned} -\hat{C}_{i33l} \ddot{\hat{a}}_l - (\hat{C}_{i13l} + \hat{C}_{i31l}) \dot{\hat{b}}_l + \hat{C}_{i11l} \hat{a}_l - \hat{\rho} \frac{\omega^2}{k^2} \hat{a}_i &= 0, \\ -\hat{C}_{i33l} \ddot{\hat{b}}_l + (\hat{C}_{i13l} + \hat{C}_{i31l}) \dot{\hat{a}}_l + \hat{C}_{i11l} \hat{b}_l - \hat{\rho} \frac{\omega^2}{k^2} \hat{b}_i &= 0, \end{aligned} \quad i = 1, 2, 3.$$

Here, the dot denotes the differentiation with respect to the variable $\tilde{x}_3 = kx_3$. With the state vectors

$$\mathbf{p} = (a_1, a_2, a_3, b_1, b_2, b_3, \dot{a}_1, \dot{a}_2, \dot{a}_3, \dot{b}_1, \dot{b}_2, \dot{b}_3)^T \in R^{12},$$

$$\hat{\mathbf{p}} = (\hat{a}_1, \hat{a}_2, \hat{a}_3, \hat{b}_1, \hat{b}_2, \hat{b}_3, \dot{\hat{a}}_1, \dot{\hat{a}}_2, \dot{\hat{a}}_3, \dot{\hat{b}}_1, \dot{\hat{b}}_2, \dot{\hat{b}}_3)^T \in R^{12},$$

the above systems can be rewritten in the normal form as follows:

$$\dot{\mathbf{p}} = A \mathbf{p}, \quad \dot{\hat{\mathbf{p}}} = \hat{A} \hat{\mathbf{p}}, \quad (19)$$

where A and \hat{A} are the corresponding matrices. Let $\lambda_1, \lambda_2, \dots, \lambda_{12}$ and $\mathbf{h}_1, \mathbf{h}_2, \dots, \mathbf{h}_{12}$ (respectively $\hat{\lambda}_1, \hat{\lambda}_2, \dots, \hat{\lambda}_{12}$ and $\hat{\mathbf{h}}_1, \hat{\mathbf{h}}_2, \dots, \hat{\mathbf{h}}_{12}$) be eigenvalues and eigenvectors of A (respectively \hat{A}). One can verify that just ℓ linear independent eigenvectors can be found for each ℓ -multiple eigenvalue. Therefore, solutions of (19) are of the form: $\mathbf{p}(x_3) = \sum_{i=1}^{12} D_i \mathbf{h}_i e^{\lambda_i k x_3}$, $\hat{\mathbf{p}}(x_3) = \sum_{i=1}^{12} \hat{D}_i \hat{\mathbf{h}}_i e^{\hat{\lambda}_i k x_3}$, where D_i and \hat{D}_i are arbitrary constants. Selecting decreasing solutions in the substrate yields:

$$\mathbf{p}(x_3) = \sum_{j=1}^N D_j \mathbf{h}_{i_j} e^{\lambda_{i_j} k x_3}, \quad \text{Re } \lambda_{i_j} > 0.$$

Note that $N \leq 6$ due to the up-down symmetry of the substrate. Solutions in the upper layer have to be of the oscillatory type:

$$\hat{\mathbf{p}}(x_3) = \sum_{j=1}^L \hat{D}_j \hat{\mathbf{h}}_{i_j} e^{\hat{\lambda}_{i_j} k x_3}, \quad \text{Re } \hat{\lambda}_{i_j} = 0.$$

Thus,

$$a_l = \sum_{j=1}^N D_j h_{ij}^{(l)} e^{\lambda_{ij} k x_3}, \quad b_l = \sum_{j=1}^N D_j h_{ij}^{(l+3)} e^{\lambda_{ij} k x_3},$$

$$\hat{a}_l = \sum_{j=1}^L \hat{D}_j \hat{h}_{ij}^{(l)} e^{\hat{\lambda}_{ij} k x_3}, \quad \hat{b}_l = \sum_{j=1}^L \hat{D}_j \hat{h}_{ij}^{(l+3)} e^{\hat{\lambda}_{ij} k x_3},$$

where l runs from 1 to 3. Therefore, the displacements u_i and \hat{u}_i , see (17) and (18), depend linearly on $D_j, j = 1, N$, and $\hat{D}_l, l = 1, L$, respectively.

For all x_1 and t , the following interface conditions must hold:

$$u_i = \hat{u}_i, \quad \text{at } x_3 = 0, \quad \text{continuity;}$$

$$C_{i3kl} \frac{\partial u_i}{\partial x_k} = \hat{C}_{ijkl} \frac{\partial \hat{u}_i}{\partial x_k}, \quad \text{at } x_3 = 0, \quad \text{equilibrium of pressures;}$$

$$\hat{C}_{ijkl} \frac{\partial \hat{u}_i}{\partial x_k} = 0, \quad \text{at } x_3 = h, \quad \text{free of forces boundary.}$$

The last system yields 18 linear equations for $N+L \leq 18$ coefficients D_j and \hat{D}_l . Note that $N+L < 18$ as a rule. Let $V = \omega/k$ be the unknown wave velocity and $G(V)$ the $18 \times (N+L)$ -matrix of the above system. Feasible wave velocities are determined from the condition of nontrivial solvability for the system $G(V)\mathbf{D} = 0$, where $\mathbf{D} = (D_1, \dots, D_N, \hat{D}_1, \dots, \hat{D}_L)^T$. Thus, the condition $\text{rank} G(V) < N+L$ holds for the feasible velocities, which is equivalent to the following condition: $\det |\bar{G}^T(V)G(V)| = 0$. The last equation can be easily solved because the computation of the left-hand-side runs very quickly even on a simple computer. Usually, three roots are being found, which corresponds to three wave types that propagate with different velocities. The selection of the desired wave type is quite obvious because the relation between their velocities is known.

Figure 5 shows the velocity profile for Love shear waves in the structure shown in Figure 4. The substrate is an ST-cut of α -quartz. The upper layer consists of amorphous quartz. The blank parts of the curve correspond to the absence of Love shear waves for these directions.

Figure 6 represents a verification of the dispersion relations method. The sensitivity of a Love wave sensor based on the structure shown in Figure 4 is being computed as $(\bar{\omega}_r - \omega_r)/\Delta m$, where $\bar{\omega}_r$ and ω_r are resonance frequencies for the loaded and unloaded sensor, respectively. The resonance frequency is defined by the equation $\lambda(\omega_r) = 40\mu\text{m}$. Here $\lambda(\omega) = 2\pi V(\omega)/\omega$ is the wave length, and $40\mu\text{m}$ is the period of the input electrodes. The loading is modeled through the adding of a 0.5nm gold layer. The computation results are in a good agreement with physical experiments described in [10].

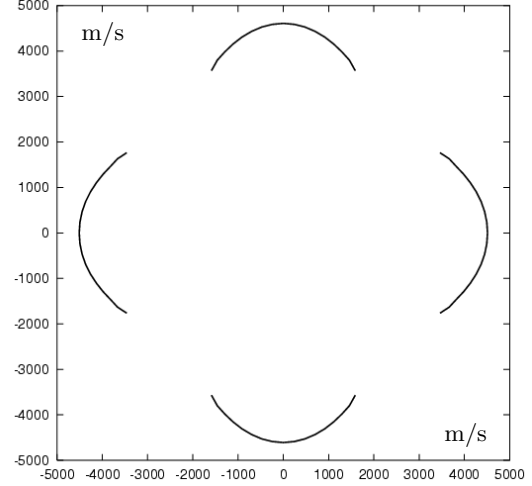


Figure 5: Velocity profile typical for structures with anisotropic substrates possessing rotation symmetries

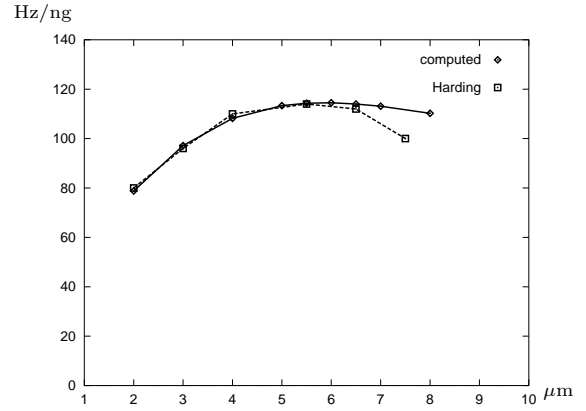


Figure 6: Comparison of numerically computed and experimentally measured sensitivities. Dependence on the thickness of the guiding (upper) layer is shown

4 Simulation Results

Now, we simulate a Love wave sensor based on the multi-layered structure shown in Figure 7. The molecular layer adhering to the surface of the auxiliary gold layer is being modeled through the homogenization technique developed in this paper. The molecular layer is expected being well described as a new material associated with equation (14). Equations (12) and (13) describe then the overlaying fluid and the underlying gold layer. Such a model allows us to compute dispersion relations which express the dependence of the velocity of Love shear waves on the excitation frequency. The sensitivity is being computed as the phase shift per surface mass loading: $2\pi\omega L(1/\bar{V} - 1/V)/(\rho\delta)$, where ω is the operating

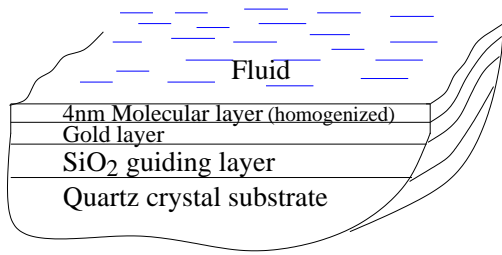


Figure 7: Multi-layered structure

frequency; L , ρ , and δ are the length, the density, and the thickness of the adhering molecular layer, respectively; \bar{V} and V are the wave velocities with and without the molecular layer, respectively.

Figure 8 represents the computed sensitivity of the Love wave sensor regarding an additional protein layer which is being adhered to the molecular aptamer layer (compare with Figure 7). The thicknesses of the adhering protein layer is equal to 43\AA .

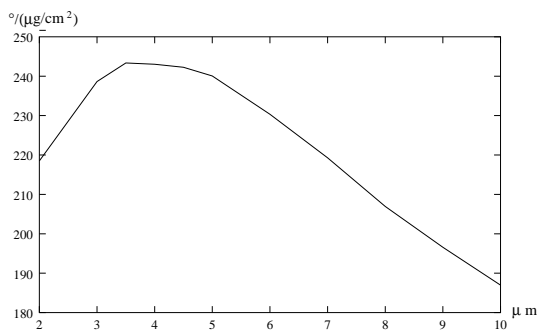


Figure 8: Sensitivity versus the thickness of the guiding layer

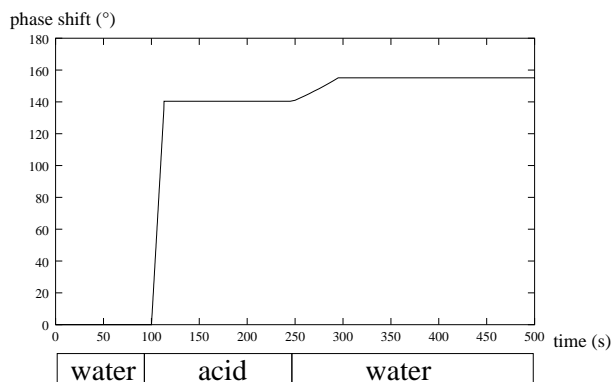


Figure 9: Modeling of the time behavior of the phase shift when etching a copper layer with an acid

Figure 9 represents the time performance of the etching process. In this case, a 9 nm copper layer was used instead of the molecular one. The water flux is being alternated with the flux of an acid solution that etches the copper layer. The phase shift is being measured. A step at the acid-to-water transition is caused by the change of the fluid viscosity. The results are in a good agreement with the measurements done in caesar laboratories.

References

- [1] N. Botkin, M. Schlensog, M. Tewes, and V. Turova, “A mathematical model of a biosensor”, *Technical Proceedings of the Fourth International Conference on Modeling and Simulation of Microsystems*, Hilton Head Island, South Caroline, USA, March 19–21, 2001, pp. 231–234.
- [2] U. Hornung, *Homogenization and porous media*, Springer, New York, 1997.
- [3] K.-H. Hoffmann and N.D. Botkin, “Homogenization of von Kármán plates excited by piezoelectric patches”, *ZAMM* **80**(9), pp. 579–590, 2000.
- [4] K.-H. Hoffmann and V.N. Starovoitov, “On a motion of a solid body in a viscous fluid. Two-Dimensional Case”, *Adv. Math. Sci. Appl.*, **9**(2), pp. 633–648, 1999.
- [5] W. Jäger and A. Micelić, “On the roughness-induced effective boundary conditions for an incompressible viscous flow”, *J. of Differential Equations*, **170**, pp. 96–122, 2001.
- [6] J.L. Lions, *Quelques méthodes de résolution des problèmes aux limites non linéaires*, Dunod Gauthier-Villars, Paris, 1969.
- [7] G. Nguetseng, “A general convergence result for a functional related to the theory of homogenization”, *SIAM J. Math. Anal.* **20**(3), pp. 608–623, 1989.
- [8] G. Allaire, “Homogenization and two-scale convergence”, *SIAM J. Math. Anal.*, **23**(6), pp. 1482–1518, 1992.
- [9] D. Lukkassen, G. Nguetseng, and P. Wall, “Two-scale convergence”, *International Journal of Pure and Applied Mathematics*, **2**(1), pp. 35–86, 2002.
- [10] G. L. Harding, “Mass sensitivity of Love-mode acoustic sensors incorporating silicon dioxide and silicon-oxy-fluoride guiding layers”, *Sensors and Actuators*, **A88**, pp. 20–28 (2001).